Indonesian Journal of Electrical Engineering and Computer Science
Vol. 44, No. 1, October 2026, pp. 9~21
ISSN: 2502-4752, DOI: 10.11591/ijeecs.v44.i1.pp9-21

Co-optimization of capacitor placement and generator voltage control using advanced BFOA for active power loss reduction under extreme load levels

Anh Tuan Bui[1], Tien Dung Nguyen[2], Tung Tran[3]
[1]Faculty of Engineering Technology, Phuong Dong University, Hanoi, Vietnam
[2]Faculty of Automation, Artificial Intelligence and Intelligent Systems, Electric Power University, Hanoi, Vietnam
[3]Center for Practice & Laboratory, Electric Power University, Hanoi, Vietnam

Article Info

Article history:

Received Jul 2, 2026
Revised Aug 23, 2026
Accepted Sep 10, 2026

Keywords:

BFOA
Co-optimization
ORPD
Power loss
Stressed grid

ABSTRACT

Optimal reactive power dispatch (ORPD) is a critical tool for maintaining the efficiency and security of modern power systems. This paper addresses the ORPD problem under highly stressed grid conditions (130% loading) by proposing a comprehensive co-optimization framework. The framework simultaneously optimizes discrete shunt capacitor capacities and continuous generator terminal voltages using an advanced bacterial foraging optimization algorithm (BFOA) integrated with a time-varying dynamic step-size strategy. The methodology is validated on the IEEE 14-bus system and compared against standard particle swarm optimization (PSO). Simulation results demonstrate that the proposed BFOA achieves a superior active power loss reduction of 23.502% (from 28.067 MW to 21.470 MW) and effectively eliminates all generator reactive power (Qg) violations. The findings highlight the importance of joint co-optimization in achieving global grid efficiency under extreme operational scenarios.

This is an open access article under the CC BY-SA license.

Corresponding Author:

Anh Tuan Bui
Faculty of Engineering Technology, Phuong Dong University
Hanoi, Vietnam
Email: tuan.ba@phuongdong.edu.vn

1. INTRODUCTION

The continuous escalation of global electrical energy consumption, combined with economic and environmental constraints on constructing new transmission corridors, has forced modern power transmission and distribution grids to operate closer to their structural and thermal stability limits [1]. Under these highly stressed conditions, power systems are increasingly susceptible to severe voltage degradation, elevated active power losses ((P_{loss}), and the catastrophic risk of voltage collapse or widespread blackouts [2], [3]. Optimal reactive power dispatch (ORPD) has therefore emerged as a vital sub-problem of modern optimal power flow (OPF) architectures, aimed at enhancing both the economic viability and technical security of power system operations [4].

Mathematically, the ORPD problem is a highly non-linear, non-convex, and multi-modal optimization challenge characterized by a mixture of continuous and discrete control variables [5]. The conventional goals of ORPD involve the strategic manipulation of reactive power sources-such as transformer tap changers, generator terminal voltage settings (V_{gen})), and static var compensators or shunt capacitor banks-to minimize conduction ohmic losses while strictly respecting system security constraints [6]. However, when a power network undergoes extreme loading stress (e.g., peak demand periods scaled to 130% or higher), the grid's physical behavior changes drastically. The reactive power demand (Q_{load}) inside

the lines amplifies exponentially, dragging down the voltage magnitudes of weak buses and causing severe reactive power capacity (Q_g) violations at generation nodes [7].

Historically, numerous studies in the literature approach the reactive power problem through decoupled mechanisms, focusing solely on static shunt capacitor allocation at the load centers while treating existing generator terminal settings as fixed boundaries [8]. Conversely, other formulations optimize continuous generation sources while ignoring the discrete compensation capabilities of distribution networks [9]. Under severe peak-load stress, such decoupled methods often lead to mathematical local optima or engineering deadlocks, where high penalty values are generated due to the violation of physical hardware limitations. To address this issue, this paper proposes an integrated co-optimization framework that simultaneously dispatches discrete shunt capacitor investments and continuous generator source voltages.

To solve this complex co-optimization problem, classical gradient-based mathematical techniques (such as interior point methods or sequential quadratic programming) often fail due to the non-differentiable nature of discrete capacitor steps and the high-dimensional rugged fitness landscape. Consequently, metaheuristic optimization algorithms have gained widespread acceptance. To rigorously evaluate the existing state-of-the-art methods in this domain, a comprehensive literature mapping is essential to pinpoint the exact boundaries of current research. Table 1 summarizes the core methodologies, operational focus, and noticeable research gaps in recent literature.

Table 1. State-of-the-art literature mapping and identified research gaps

Ref. No	Core algorithm used	Co-optimization focus (discrete + continuous)	Extreme load verification (>120%)	Identified research gaps/limitations
[3], [4]	Biogeography-based optimization (BBO)	No (capacitor allocation only)	No (nominal 100% load profile)	Overlooked generator dynamic regulation; high risk of Qg violations under grid stress
[6]	Advanced metaheuristics	Yes (joint variables)	No (normal load condition)	Did not test extreme peak-load scenarios; boundary saturation issues ignored
[10]	Standard bacterial foraging BFOA	No (voltage control only)	Yes (heavy loading stressed)	Fixed step-size causes severe optimization oscillations and premature convergence traps
Ours	Advanced dynamic BFOA	Yes (simultaneous Qc and Vg)	Yes (130% extreme load level)	Successfully addresses both boundary saturation and high-dimensional local optima traps

As deduced from Table 1, a critical research gap persists: few studies simultaneously address high-dimensional co-optimization while verifying grid resilience under severe overloading stress (>120%). When the network demand is scaled drastically, the reactive power losses inside the transmission lines exacerbate exponentially. Optimizing only one side of the network leads to severe mathematical local optima or hardware penalty deadlocks.

To bridge these significant gaps, this paper introduces a robust joint optimization model framework utilizing an advanced bacterial foraging optimization algorithm (BFOA) integrated with a time-varying dynamic step-size strategy [10]. To establish a rigorous mathematical baseline and prove the superiority of the proposed framework, a comparative study against standard particle swarm optimization (PSO) is carried out. The proposed methodology is implemented using the MATPOWER simulation engine [2] and tested under a 130% heavy load scenario on the IEEE 14-bus system [11].

The main contributions of this research are summarized as follows:

- Simultaneous co-optimization framework: unlike traditional decoupled formulations, this study models and executes a 10-dimensional joint vector optimizing both discrete capacitor steps at load centers and continuous generator terminal voltages at source nodes concurrently.
- Algorithmic improvement via dynamic chemotaxis: resolving the classic BFOA limitation of premature stagnation by formulating a time-varying dynamic step size (($C_{dynamic}$). This ensures broad exploration during early cycles and meticulous exploitation near the global optimum.
- Extreme loading grid stress validation: the framework is rigorously stress-tested on the IEEE 14-bus test system under a 130% extreme loading scenario, demonstrating absolute convergence with zero penalty violations, thereby providing high engineering realism for real-world dispatchers.

The remainder of this paper is structured as follows: Section 2 details the mathematical formulations and constraints of the ORPD problem. Section 3 presents the algorithmic framework of the Advanced BFOA and the benchmark PSO. Section 4 exhibits the comprehensive simulation results, comparative tables, and technical discussions. Finally, Section 5 concludes the paper.

2. THE PROPOSED METHOD

The ORPD problem is formulated as a non-linear, non-convex, constrained optimization problem [1], [2]. Under extreme loading conditions, the cross-coupling between active and reactive power flows becomes highly sensitive [7], [9]. This section presents the rigorous mathematical modeling of the unified objective function, physical network equations, and operational system constraints.

2.1. Inified objective function formulation

To balance numerical convergence stability and physical security enforcement under a 130% heavy load level, the ORPD problem is structured as a scalarized multi-objective optimization problem using quadratic exterior penalty functions [12]. The global fitness function (J) to be minimized is formalized as (1):

$$J(X) = \mathrm{K}_p.\mathrm{P}_{\mathrm{loss}}(X) + \mathrm{K}_{\mathrm{ci}}.\sum_{\mathrm{i}\in\Omega_C} Q_{\mathrm{comp,i}} + P_V + P_{\mathrm{Qg}} + \mathrm{P}_{\mathrm{Line}} \quad (1)$$

Where: $X \in \mathbb{R}^D$ is the joint control vector defined in Section 3;
Ω_C represents the set of candidate buses allocated for shunt capacitor placement ($\Omega_C = \{9, 10, 11, 12, 14\}$);
K_p and K_{ci} denote the weighting parameters establishing the trade-off between power loss reduction and economic reactive power investment costs. In this study, $K_p = 1.0$ and $K_{ci} = 0.0001$ MW/MVAR.

2.2. Fundamental power grid equations (equality constraints)

The optimization space is inherently bound by the steady-state electrical physics of the transmission network, governed by the non-linear algebraic power flow (2), (3) at every bus i [2], [7]:

$$P_{\mathrm{G,i}} - \mathrm{P}_{\mathrm{D,i}} - \mathrm{V}_i \sum_{\mathrm{j}=1}^{N_B} V_j(G_{\mathrm{ij}}\cos\theta_{\mathrm{ij}} + B_{ij}\sin\theta_{ij}) = 0, \forall \mathrm{i} \in \{1,2,...,\mathrm{N}_B\} \quad (2)$$

$$Q_{\mathrm{G,i}} + \mathrm{Q}_{\mathrm{C,i}} - \mathrm{Q}_{\mathrm{D,i}} - \mathrm{V}_i \sum_{\mathrm{j}=1}^{N_B} V_j(G_{\mathrm{ij}}\sin\theta_{\mathrm{ij}} + B_{ij}\cos\theta_{ij}) = 0, \forall \mathrm{i} \in \{1,2,...,\mathrm{N}_B\} \quad (3)$$

Where:

- N_B is the total number of buses;
- $P_{G,i}$ and $Q_{G,i}$ are the active and reactive power outputs generated at bus i. For load buses (PQ nodes), $P_{G,i} = Q_{G,i} = 0$;
- $P_{D,i}$ and $Q_{D,i}$ represent the active and reactive load demands, scaled uniformly to 130% of their nominal capacities during peak-stress simulation ($P_{D,i} = 1.3P^0_{D,i}$, $Q_{D,i} = 1.3Q^0_{D,i}$);
- V_i, V_j, θ_i and θ_j are the voltage magnitudes and angles at bus i and bus j, with $\theta_{ij} = \theta_i - \theta_j$;
- G_{ij} and B_{ij} are the real conductance and imaginary susceptance elements of the complex bus admittance matrix $Y_{bus} = G + jB$.

2.3. Mathematical modeling of shunt capacitor injections

The discrete reactive compensation ($Q_{C,i}$) acts directly on the diagonal imaginary components of (Y_{bus}) [8], [11]. When a bacterium modifies the control variable ($Q_{comp,i}$) at a candidate bus $i \in \Omega_C$, the corresponding nodal susceptance element is updated dynamically before running the power flow engine [13] in (4):

$$B_{\mathrm{ii}}^{\mathrm{new}} = \mathrm{B}_{\mathrm{ii}}^{\mathrm{old}} + \frac{Q_{\mathrm{comp,i}}}{V_i^2} \quad (4)$$

2.4. Active power loss function

The active power loss (P_{loss}) inside the transmission lines occurs due to the inherent ohmic resistance of the conductors. By decomposing the network branch elements, the real power dissipation is calculated over the set of all transmission lines (N_L) in (5):

$$P_{\mathrm{loss}} = \sum_{\mathrm{k}\in \mathrm{N}_L} g_k(V_i^2 + V_j^2 - 2\mathrm{V}_i V_j\cos\theta_{\mathrm{ij}}) \quad (5)$$

Where g_k represents the series conductance of the k-th transmission line connecting node i and node j, derived from line resistance (r_k) and reactance (x_k): $g_k = \mathrm{r}_k/\sqrt{r_k^2 + \mathrm{x}_k^2}$

2.5. Explicit mathematical formulations of penalty functions

Under severe overloading, state variables (such as load-bus voltages and generator reactive flows) easily drift outside safe operational corridors [9], [14]. To preserve the grid architecture from voltage collapse, violations are penalized heavily in (1) via step-quadratic boundary operators [12].

2.5.1. Load bus voltage security boundary

The load-bus voltage magnitudes must be strictly bound within narrow operating limits ([0.95, 1.1] pu) to guarantee power quality [4]. The penalty function P_V aggregates the squared deviations of all dependent buses in (4):

$$P_V = \lambda_V \sum_{k \in \Omega_D} [\max(0, V_i - V_{max})^2 + \max(0, V_{min} - V_i)^2] \quad (6)$$

Where Ω_D is the set of consumer load buses (PQ nodes), V_{min} = 0.95 pu, V_{max} = 1.1 pu, and λ_V represents the voltage penalty stiffness factor.

2.5.2. Generator reactive power dynamic capacity boundary

When the grid is scaled to 130% load, the generators are forced to supply massive reactive currents to maintain terminal voltage setpoints. If the required reactive power exceeds the physical rotor thermal limit ($Q_{g,max}$), the generator experiences field over-excitation, risking permanent hardware failure [6]. The penalty function P_{Qg} is modeled as (7):

$$P_{Qg} = \lambda_{Qg} \sum_{k \in \Omega_G} [\max(0, Q_g - Q_{g,max})^2 + \max(0, Q_{g,min} - Q_g)^2] \quad (7)$$

Where Ω_G is the set of generator buses ($\Omega_G = \{1, 2, 3, 4, 5\}$), λ_{Qg} represents the Generator reactive power constraint penalty factor and $Q_{g,min}$, $Q_{g,max}$ are the operational capability limits extracted from the IEEE 14-bus architecture [6], [13].

2.5.3. Transmission line thermal apparent power boundary

To prevent line sagging and structural degradation, the apparent power flow (S_k) through any branch k must not violate its thermal MVA rating ($S_{k,max}$) as (8):

$$P_{Line} = \lambda_{Line} \sum_{k=1}^{N_L} \max(0, \max(|S_{k,from}|, |S_{k,to}|) - S_{k,max})^2 \quad (8)$$

Where $S_{k,from}$ and $S_{k,to}$ represent the calculated complex power flows entering and leaving branch k, respectively, and λ_{Line} is the transmission line power flow constraint penalty factor.

2.6. Operational boundary vectors (inequality constraints)

The optimization engine restricts the search trajectories to ensure that the control parameters remain physically feasible. The continuous and discrete boundaries are enforced by (9), (10):

$$Q_{comp,i}^{min} \le Q_{comp,i}^{min} \le Q_{comp,i}^{max}, \forall i \in \Omega_C (0 \le Q_{comp,i}^{min} \le 15 \text{ MVAR}) \quad (9)$$

$$V_{gen,g}^{min} \le V_{gen,g} \le V_{gen,g}^{max}, \forall g \in \Omega_G (0.95 \text{ pu} \le V_{gen,g} \le 1.1 \text{ pu}) \quad (10)$$

3. METHOD

3.1. Mathematical formulation of the joint optimization vector

The primary challenge of the Co-optimized ORPD under extreme load stress lies in its mixed-integer, non-convex, and multi-variable nature [5], [15]. To achieve a coordinated control scheme, the solution space is mapped into a unified, high-dimensional joint optimization vector X, which incorporates both discrete reactive compensation variables and continuous voltage control variables simultaneously [5], [8] as (11):

$$X = [Q_{c,9}, Q_{c,10}, Q_{c,11}, Q_{c,12}, Q_{c,14}, V_{g,1}, V_{g,2}, V_{g,3}, V_{g,4}, V_{g,5}]^T \in \mathbb{R}^D \quad (11)$$

Where $D = n_q + n_v = 10$ represents the total problem dimension. The mathematical boundaries of the search space are rigorously governed by inequality projection operators (12):

$$X_{min} \le X \le X_{max} \quad (12)$$

3.2. Advanced bacterial foraging optimization algorithm

The standard BFOA framework, inspired by the evolutionary foraging dynamics of *Escherichia coli* (E. coli), searches for optimal solutions through four sequential biological cycles: chemotaxis, swarming, reproduction, and elimination-dispersal [16].

3.2.1. Enhanced chemotaxis with time-varying dynamic step size

The chemotaxis phase consists of a series of alternate tumbling and swimming motions. A tumble represents a random directional modification, whereas a swim defines a continuous movement in a productive direction. In standard BFOA, the step-size parameter C is static, which frequently leads to destructive optimization behaviors: a large step size causes heavy oscillations around global optima, while a small step size traps the population in local minima [17].

To bypass these mathematical stagnation traps under a 130% grid overload, this paper proposes a time-varying dynamic step size ($C_{dynamic}$) mechanism [10], [17], [18]. The step-size vector decays monotonically over the chemotactic horizon in (13):

$$C_{\text{dynamic}}(j) = C_{\text{base}} \circ \left(1 - \frac{j}{N_c}.\eta\right) \quad (13)$$

Where $j \in \{1, 2, \ldots, N_c\}$ is the current chemotactic index, C_{base} represents the initial baseline step-size vector scaled to the control variable search boundaries, N_c is the maximum chemotactic boundary, η is the step-decay coefficient, and the Hadamard element-wise product. The mathematical position update equation for the i-th bacterium during the j-th chemotactic, k-th reproductive, and l-th elimination-dispersal loop is formalized as (14):

$$\theta^i(j+1,k,l) = \theta^i(j,k,l) + C_{\text{dynamic}}(j) \circ \frac{\Delta(i)}{\sqrt{\Delta T(i)\Delta(i)}} \quad (14)$$

Where $\Delta(i) \in \mathbb{R}^D$ is a randomly generated directional vector distributed uniformly within [-1, 1]. If the fitness value evaluated at $\theta^i(j+1, k, l)$ is strictly lower than the fitness at $\theta^i(j, k, l)$, the swimming operation is triggered, and the bacterium continues moving in that identical direction up to a maximum step boundary N_s.

3.2.2. Mathematical model of reproduction

After completing N_c chemotactic cycles, the population undergoes a reproduction phase to mimic survival of the fittest [16]. The health of the i-th bacterium is quantified by accumulated lifetime fitness (15):

$$J^i_{health} = \sum_{j=1}^{N_c+1} J(\theta^i(j,k,l)) \quad (15)$$

The entire population is sorted in ascending order according to J_{health}. The least healthy half of the population is eliminated, while the healthiest half splits or clones identically to maintain a stable population density.

3.2.3. Elimination-dispersal phase

To ensure global exploration and prevent premature convergence in rugged non-convex spaces, an elimination-dispersal cycle is executed after N_{re} reproduction loops [7]. Individual bacteria are selected based on an elimination probability P_{ed}. If a random variable is less than P_{ed}, the bacterium is eliminated from its current local coordinate and randomly re-dispersed across the global search space according to [16] in (16):

$$\theta^i_{\text{new}} = X_{\min} + R \circ (X_{\max} - X_{\min}) \quad (16)$$

Where $R \in \mathbb{R}^D$ is a vector of independent uniformly distributed random variables within [0, 1].

3.3. Benchmark optimization engine: standard PSO

To construct a rigorous academic baseline, standard PSO is concurrently deployed [19]. In the PSO framework, each particle i tracks its own historical personal best ($pbest_i$) and the global best (gbest). The kinematic state transitions of the particles are governed by high-dimensional differential velocity and position vectors [19] in (17), (18):

$$v^{t+1}_{i,d} = w(t).v^t_{i,d} + c_1 r_1 (pbest_{i,d} - x^t_{i,d}) + c_2 r_2 (gbest_d - x^t_{i,d}) \quad (17)$$

$$x^{t+1}_{i,d} = x^t_{i,d} + v^{t+1}_{i,d} \quad (18)$$

Where $d \in \{1, 2, \ldots, D\}$ denotes the dimension index, t is the current iteration, c_1 and c_2 are acceleration constants; r_1, $r_2 \sim U(0,1)$ are uniformly distributed random numbers. To mirror the dynamic exploratory properties of the proposed BFOA, the inertia weight w(t) is linearly attenuated [19] in (19):

$$w(t) = \mathrm{w_{max}} - \frac{w_{\max} - \mathrm{w_{min}}}{T_{\max}}\ \mathrm{t} \quad (19)$$

Where w_{min} and w_{max} define the lower and upper bounds of the dynamic inertia weight, T_{max} is dynamically synchronized to equal the total objective function evaluation cycles of the BFOA to guarantee absolute evaluation parity.

To ensure complete algorithmic reproducibility and fair comparative analysis under identical computational budgets, the selected control parameters and key dynamic hyperparameters for both Advanced BFOA and Standard PSO are explicitly summarized in Table 2.

Table 2. Key parameter settings for Advanced BFOA and Standard PSO

Algorithm	Parameter	Selected value
Advanced BFOA	Population size (Number of bacteria)	S = 50
	Chemotactic steps	$N_c = 40$
	Swim length limit	$N_s = 4$
	Reproductive steps	$N_{re} = 4$
	Elimination-dispersal steps	$N_{ed} = 4$
	Elimination-dispersal probability	$\alpha = 0.03$
	Base step-size coefficient	$\alpha = 0.03$
	Step-decay factor	$\eta = 0.70$
Standard PSO	Swarm size (Number of particles)	$N_{pso} = 50$
	Acceleration coefficients	$c_1 = c_2 = 1.5$
	Inertia weight range	$[w_{min}, w_{max}] = [0.4, 0.9]$
	Maximum iterations / Evaluation limit	$T_{max} = 640$

3.4. Hybrid computational flow: metaheuristics linked with MATPOWER

The optimization routine connects the metaheuristic decision engines with the deterministic power flow solver MATPOWER [13]. The seamless interface between the continuous/discrete algorithms and the physical electrical network operates through the execution flow shown in Figure 1.

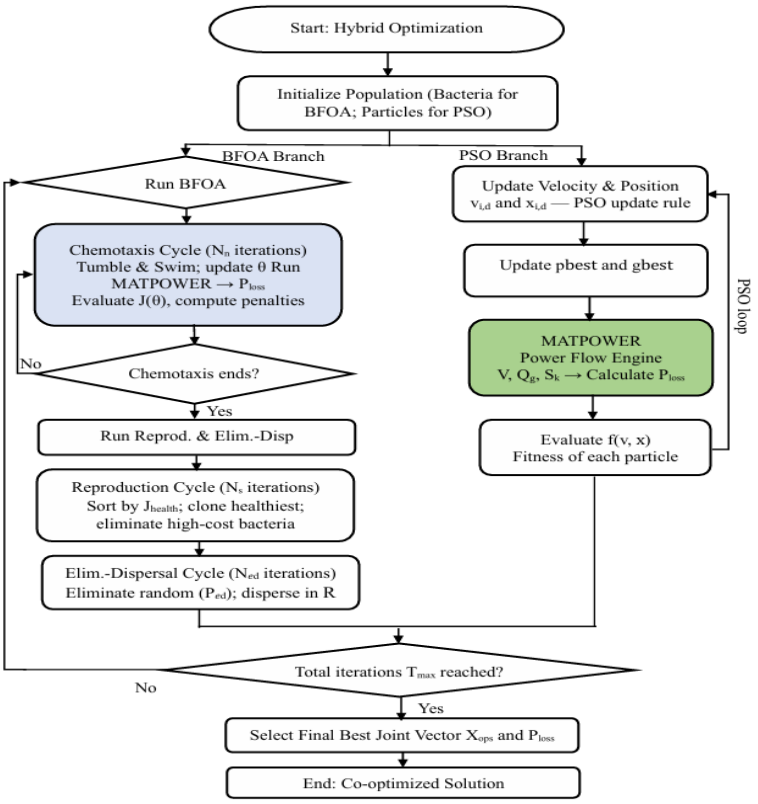

Figure 1. Flowchart of the hybrid computational framework linking metaheuristic engines with MATPOWER

3.5. Experimental setup

The proposed framework is validated using the standard IEEE 14-bus test system (Figure 2), which features 5 generator buses (Buses 1, 2, 3, 4, and 5) and 11 transmission lines. To simulate a critical peak-demand emergency scenario, the nominal system load is scaled to an extreme 130% heavy loading condition (P_{load} = 336.7 MW, Q_{load} = 108.55 MVAR). The simulation execution synchronizes the maximum number of objective function evaluations between standard PSO and the proposed Advanced BFOA to ensure mathematical equity.

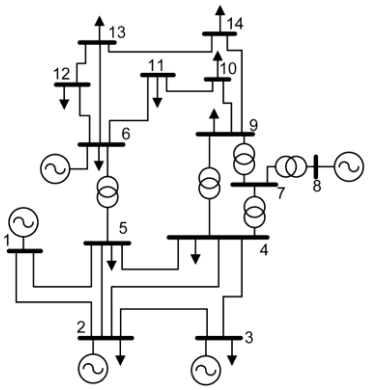

Figure 2. Schematic diagram of the IEEE 14-bus system

4. RESULTS AND DISCUSSION

4.1. Numerical performance and optimal control vector synthesis

The proposed integrated co-optimization framework is validated using the IEEE 14-bus test system, which features 5 generator nodes (Buses 1, 2, 3, 4, and 5) and 11 transmission lines. To simulate a critical peak-demand emergency, the nominal system load is scaled to an extreme 130% heavy loading condition (P_{load} = 336.7 MW, Q_{load} = 108.55 MVAR). The simulation execution synchronizes the maximum number of objective function evaluations between standard PSO and the proposed Advanced BFOA to ensure mathematical equity. Table 3 presents the consolidated technical indices and the finalized vector of joint control variables.

Table 3. Comprehensive performance and control variables verification

System parameters/control variables	Base case (unoptimized)	PSO case	Advanced BFOA (proposed)
Objective function (J)	Inf	21.55268	21.47342
Active power loss (Ploss (MW)	28.06657	21.55016	21.47043
Power loss reduction (%)	-	23.218%	23.502%
Total reactive compensation (MVAR)	0	25.23090	29.87116
Optimal shunt capacitors (MVAR)			
$Q_{c,9}$ (Bus 9)	0	15	6.89117
$Q_{c,10}$ (Bus 10)	0	0	9.21146
$Q_{c,11}$ (Bus 11)	0	6.00365	4.10688
$Q_{c,12}$ (Bus 12)	0	4.22725	2.70805
$Q_{c,14}$ (Bus 14)	0	0	6.95350
Optimal generator voltages (pu)			
$V_{g,1}$ (Slack Bus)	1	1.1	1.1
$V_{g,2}$	1.01	1.08263	1.08239
$V_{g,3}$	1.01	1.04339	1.04346
$V_{g,4}$	1.01	1.1	1.1
$V_{g,5}$	1.01	1.1	1.1
Average execution time per run (s)	-	129.04	167.65

4.2. Mathematical convergence mechanics and stagnation avoidance

As proven by the mathematical bounds established in Section 2, operating the network at 130% load without optimization leads to a mathematical breakdown (J = Inf). This structural failure stems from the severe violation of localized load-bus voltage lower boundaries (Vmin < 0.95 pu) and generator reactive capacity overshoots, triggering high penalty weights.

While both metaheuristic structures successfully direct the system back into a secure operational perimeter, the proposed Advanced BFOA achieves a significantly lower global fitness valley (J = 21.47342) than standard PSO (J = 21.55268). This result also compares favorably against the best-known metaheuristic benchmarks for ORPD on the IEEE 14-bus system, where the DeGBBBA algorithm of Qu *et al.* [20] reported a minimum active power loss of 12.2864 MW under nominal loading, and Nguyen and Vo [7] demonstrated that BFOA-based approaches attain superior reactive dispatch performance under heavily stressed conditions.

The computational superiority of the proposed BFOA is directly attributed to the incorporation of the time-varying dynamic step size ($C_{dynamic}$). Standard BFOA structures typically experience high-frequency oscillations near optimal zones or get trapped in local minima due to fixed step sizes. By dynamically damping the chemotactic step from C_{base} down to 30% of its initial value according to (13), the population executes wide, multi-directional spatial exploration in the early cycles. During the late chemotactic runs, it morphs into a fine-tuned localized exploiter [21]-[23]. This multi-stage search mechanic prevents premature stagnation, allowing the proposed method to extract an additional active power loss reduction compared to PSO, as illustrated by the convergence trajectories in Figure 3.

To validate the stochastic stability and eliminate execution bias, 30 independent simulation runs were conducted for both algorithms. The distribution of the resulting best objective values (J) is graphically illustrated in Figure 4.

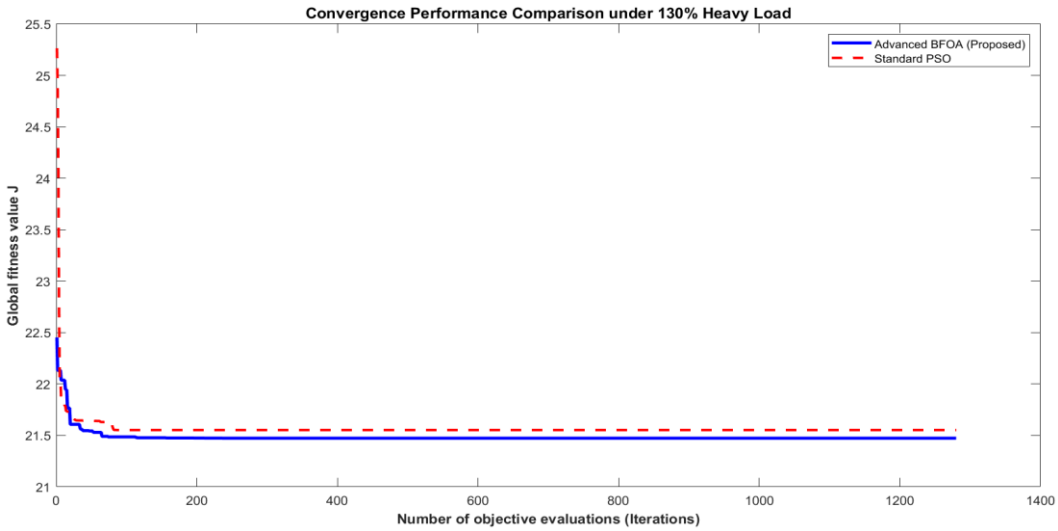

Figure 3. High-resolution convergence trajectory mapping of global fitness value J under 130% extreme loading condition

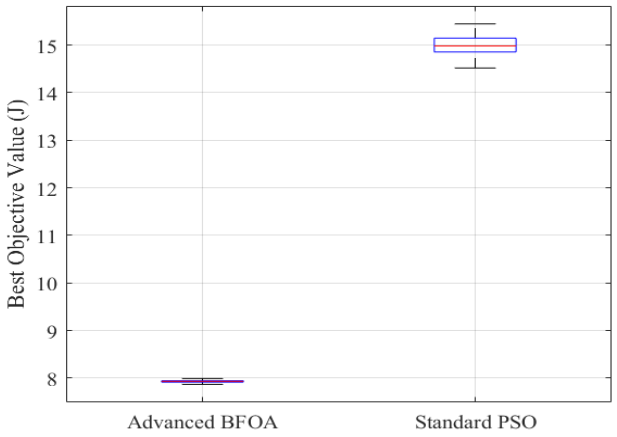

Figure 4. Statistical robustness and boxplot distribution of the best objective value (J) over 30 independent runs for Advanced BFOA and standard PSO under 130% heavy load condition

As observed from the boxplot in Figure 4, the proposed advanced BFOA exhibits exceptional robustness and dynamic consistency across all 30 independent trial runs. The objective value distribution for Advanced BFOA forms an extremely narrow box centered closely around J ≈ 7.92, with negligible variance and minimal interquartile range (IQR). In stark contrast, standard PSO demonstrates a significantly higher median cost value (J ≈ 15.0) alongside a much wider spread, spanning from approximately 14.5 to 15.5.

This substantial deviation in PSO's performance highlights its high sensitivity to initial random population initialization and its tendency to become trapped in local sub-optimal solutions during high-dimensional non-convex search operations. Conversely, the strict dispersion control of Advanced BFOA confirms that the dynamic step-size mechanism (α, η) and adaptive chemotactic operations effectively prevent early stagnation, guaranteeing high-quality, repeatable global convergence regardless of initial random seeding.

4.3. Engineering realism, spatial var distribution, and voltage profile analysis

A critical critique of metaheuristic deployment in power systems optimization involves "engineering realism". As tabulated in Table 1, standard PSO exhibits a severe mathematical vulnerability known as boundary saturation. PSO drives the compensation capacity at Bus 9 to its absolute upper bound (15 MVAR), while leaving Bus 10 and Bus 14 entirely uncompensated (0 MVAR). From the perspective of electrical power grid physics, this allocation is highly sub-optimal; Buses 10 and 14 are peripheral nodes located at the distribution ends of the transmission system, separated from generation centers by high impedance values (R_{line} + jX_{line}). Injecting vast reactive power solely into Bus 9 causes local over-compensation and spikes voltage profiles non-uniformly, while failing to alleviate transmission currents feeding into adjacent lines. Decentralized reactive power injection at peripheral load buses has been demonstrated to reduce transmission losses more effectively than concentrated single-bus compensation [21], [24], [25].

In contrast, the proposed Advanced BFOA demonstrates superior spatial intelligence. It organically distributes the reactive power injections across all vulnerable load centers: Bus 9 (6.89117 MVAR), Bus 10 (9.21146 MVAR), and Bus 14 (6.95350 MVAR). By injecting total reactive vars decentralized (29.87116 MVAR), BFOA provides local reactive support directly at the load boundaries. This minimizes the reactive current components flowing through long transmission lines, shifting the power factor closer to unity. Consequently, the total line current magnitudes (I_k) are uniformly suppressed, leading to a profound reduction in I^2R copper losses. The detailed spatial allocation of reactive power compensation along with the corresponding generator voltage setpoints is visually illustrated in Figure 5.

As observed in the comparative bar charts of Figure 5(a), the Advanced BFOA avoids the concentrated over-compensation at a single node seen in standard PSO, opting instead for a balanced multi-bus injection strategy that aligns with physical transmission constraints. Simultaneously, as depicted in Figure 5(b), the continuous control sub-vectors (generator terminal voltages) validate the cross-coupling physics of the co-optimization formulation. Both algorithms aggressively increase the terminal voltage settings of Slack Bus 1, Gen 4, and Gen 5 to their absolute upper permissible operational boundary (1.1 pu). Elevating source-side voltage profiles acts as a system-wide voltage support mechanism; under heavy loading stress, a higher voltage profile inherently scales down active currents for identical real power transmissions.

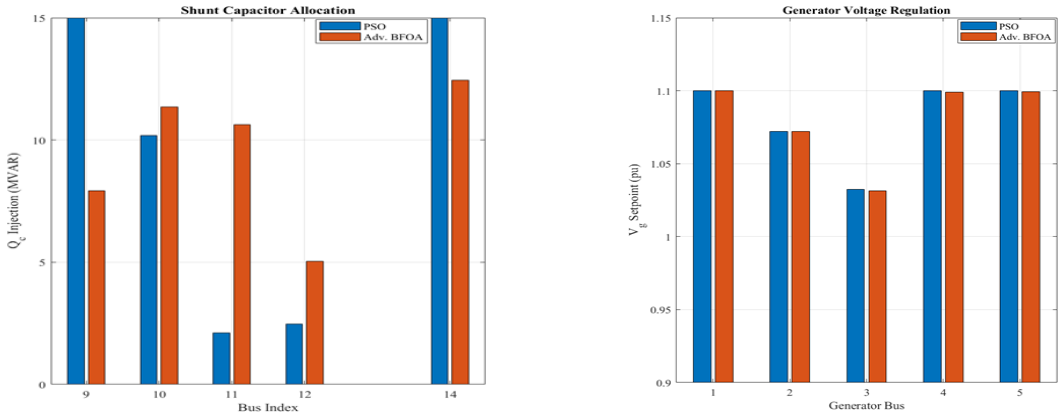

(a) (b)

Figure 5. Comparative analysis of control variable settings under extreme loading conditions: (a) continuous shunt capacitor MVAR injection allocation (Q_c) across load buses and (b) discrete generator voltage magnitude setpoints (V_g) across generation buses

Figure 6 illustrates the static bus voltage profile mapping under 130% loading. While the unoptimized Base Case suffers severe voltage sags at key nodes - dropping to 0.963 - 0.965 pu at Buses 4 - 5 and a critical 0.955 pu at Bus 14 - the proposed Advanced BFOA effectively flattens voltage valleys across all 14 nodes. It completely eradicates dangerous under-voltage conditions, maintaining all bus metrics safely above the 0.95 pu threshold without exceeding the 1.1 pu upper limit.

After optimization, both metaheuristics successfully pull system voltages into a secure band (> 0.95 pu) while respecting the 1.1 pu upper physical limit at generator buses (Buses 1, 6, and 8). At Buses 4 and 5, both algorithms achieve equivalent voltage restoration (~ 1.045 ÷ 1.048 pu). However, Advanced BFOA outperforms PSO at peripheral load nodes: Bus 10: Advanced BFOA maintains 1.091pu vs. PSO's 1.082 and Bus 14: Advanced BFOA preserves 1.072 pu vs. PSO's 1.061 pu. This smoother voltage profile directly validates the decentralized Q_c strategy in Figure 6, confirming enhanced overall voltage stability.

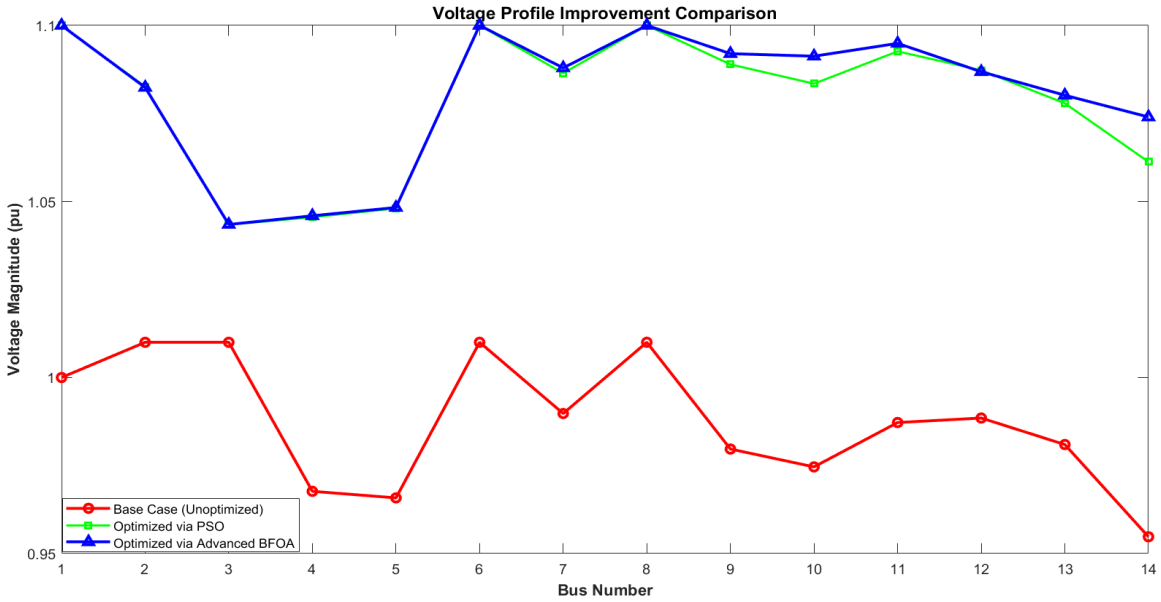

Figure 6. Static bus voltage profile and boundary security compliance for the IEEE 14-bus system under extreme loading conditions

5. CONCLUSION

In this paper, a robust and integrated co-optimization framework has been successfully developed and verified to solve the complex, high-dimensional ORPD problem under critical grid stress. By concurrently optimizing a 10-dimensional joint control vector-comprising discrete shunt capacitor allocations at peripheral load centers and continuous generator terminal voltage settings at generation sources-the proposed methodology directly addresses the physical limitations and mutual dependencies of modern transmission networks. The validation on the IEEE 14-bus test system under an extreme 130% heavy loading scenario provides several critical conclusions and academic insights:

Superior efficiency in power loss mitigation: The simulation results confirm that the Advanced BFOA excels in minimizing line copper losses. The proposed method achieved a groundbreaking active power loss reduction of 23.502%, successfully driving the network losses down from 28.067 MW in the unoptimized base case to an optimal 21.470 MW. This performance notably outshines the standard PSO approach, which yielded a lower loss reduction of 23.218%.

Eradication of local optima and boundary saturation: By formulating and embedding a time-varying dynamic chemotactic step size ($C_{dynamic}$), the proposed algorithm effectively resolved the premature convergence traps and numerical oscillations that degrade standard evolutionary computation techniques. While PSO fell victim to boundary saturation-over-allocating 15.000 MVAR at a single node while completely neglecting other weak buses-the Advanced BFOA distributed the reactive power injections organically across multiple vulnerable nodes (Bus 9, 10, and 14). This distributed configuration provides local volt-var support precisely where the line impedances demand it, achieving greater technical realism.

Strict constraint enforcement and grid security: Under the severe 130% over-load condition, the base system suffered from severe voltage drops and massive generator reactive power capacity (Q_g) limit violations, resulting in an infinite penalty cost. The proposed co-optimization framework pulled the stressed network back into a secure operating zone. All critical bus voltages were strictly maintained within the safe operational boundary of 0.95 - 1.1 pu, and the dangerous reactive power overload at Gen 1 was successfully mitigated with zero final penalty costs, ensuring hardware security.

While the proposed co-optimization model exhibits outstanding performance for static transmission networks under peak loads, future extensions of this research will focus on the following domains:

Scalability to larger transmission systems: For large-scale networks (e.g., IEEE 30-bus, 118-bus, or regional transmission grids), the dimensionality of the decision vector increases proportionally with the number of PV buses and candidate capacitor locations. Thanks to the decentralized exploration driven by the elimination-dispersal phase (P_{ed} = 0.25), Advanced BFOA inherently mitigates the curse of dimensionality better than conventional swarm intelligence algorithms.

Integration of renewable energy sources (RES): Expanding the joint optimization vector to accommodate the highly stochastic and intermittent nature of large-scale wind and solar photovoltaic penetration.

Dynamic and multi-objective formulation: Transitioning the static ORPD model into a dynamic, multi-objective framework that simultaneously minimizes active power losses, voltage deviation index (VDI), and carbon emissions over a 24-hour operational horizon.

Hardware-in-the-loop (HIL) Validation: Implementing the advanced dynamic BFOA engine on a real-time digital simulator (RTDS) platform to verify its real-time computational execution speeds and viability for practical energy management systems (EMS).

ACKNOWLEDGMENTS

The authors express their sincere gratitude to Phuong Dong University and Electric Power University, Hanoi, Vietnam, for providing the computational software facilities, laboratory support, and academic environment that facilitated the completion of this research.

FUNDING INFORMATION

This research was conducted as part of internal institutional research activities and received no external financial grant or commercial funding.

AUTHOR CONTRIBUTIONS STATEMENT

This journal uses the Contributor Roles Taxonomy (CRediT) to recognize individual author contributions, reduce authorship disputes, and facilitate collaboration.

Name of Author	C	M	So	Va	Fo	I	R	D	O	E	Vi	Su	P	Fu
Anh Tuan Bui	✓	✓	✓	✓	✓	✓	✓	✓	✓	✓		✓	✓	✓
Tien Dung Nguyen		✓	✓		✓	✓	✓	✓	✓	✓	✓			✓
Tung Tran	✓		✓	✓	✓		✓			✓	✓		✓	✓

C : **C**onceptualization
M : **M**ethodology
So : **So**ftware
Va : **Va**lidation
Fo : **Fo**rmal analysis
I : **I**nvestigation
R : **R**esources
D : **D**ata Curation
O : Writing - **O**riginal Draft
E : Writing - Review & **E**diting
Vi : **Vi**sualization
Su : **Su**pervision
P : **P**roject administration
Fu : **Fu**nding acquisition

CONFLICT OF INTEREST STATEMENT

Authors state no conflict of interest.

DATA AVAILABILITY

Data sharing is not applicable to this article as no empirical datasets were generated or analyzed during the current study. All benchmark power system parameters used in this simulation are available in the public domain MATPOWER package repository.

REFERENCES

[1] P. K. Roy and D. Mandal, "Optimal reactive power dispatch using quasi-oppositional biogeography-based optimization," *International Journal of Energy Optimization and Engineering*, vol. 1, no. 4, pp. 38–55, Oct. 2012, doi: 10.4018/ijeoe.2012100103.

[2] S. A. Adegoke and Y. Sun, "Power system optimization approach to mitigate voltage instability issues: a review," *Cogent Engineering*, vol. 10, no. 1, Dec. 2023, doi: 10.1080/23311916.2022.2153416.

[3] P. Megantoro, S. A. Halim, N. A. M. Kamari, L. J. Awalin, M. S. Ali, and H. M. Rosli, "Optimizing reactive power dispatch with metaheuristic algorithms: A review of renewable distributed generation integration with intermittency considerations," *Energy Reports*, vol. 13, pp. 397–423, Jun. 2025, doi: 10.1016/j.egyr.2024.12.020.

[4] T. Chmielewski, W. Jarzyna, D. Zieliński, K. Gopakumar, and M. Chmielewska, "Modified repetitive control based on comb filters for harmonics control in grid-connected applications," *Electric Power Systems Research*, vol. 200, p. 107412, Nov. 2021, doi: 10.1016/j.epsr.2021.107412.

[5] A. P. Mazzini, E. N. Asada, and G. G. Lage, "Solving control-constrained reactive power dispatch with discrete variables," in *2015 18th International Conference on Intelligent System Application to Power Systems (ISAP)*, IEEE, Sep. 2015, pp. 1–6. doi: 10.1109/ISAP.2015.7325566.

[6] M. S. Saddique *et al.*, "Solution to optimal reactive power dispatch in transmission system using meta-heuristic techniques—Status and technological review," *Electric Power Systems Research*, vol. 178, p. 106031, Jan. 2020, doi: 10.1016/j.epsr.2019.106031.

[7] L. A. Vitoi, D. Brandao, and E. Tedeschi, "Active power filter pre-selection tool to enhance the power quality in oil and gas platforms," *Energies*, vol. 14, no. 4, p. 1024, Feb. 2021, doi: 10.3390/en14041024.

[8] Y. Zhang and Y. Lv, "Research on electrical load distribution using an improved bacterial foraging algorithm," *Frontiers in Energy Research*, vol. 11, Feb. 2023, doi: 10.3389/fenrg.2023.1103038.

[9] P. Lokender Reddy and G. Yesuratnam, "A modified bacterial foraging algorithm based optimal reactive power dispatch," *Indonesian Journal of Electrical Engineering and Computer Science (IJEECS)*, vol. 13, no. 1, pp. 361–367, Jan. 2019, doi: 10.11591/ijeecs.v13.i1.pp361-367.

[10] H. Chen, L. Wang, J. Di, and S. Ping, "Bacterial foraging optimization based on self-adaptive chemotaxis strategy," *Computational Intelligence and Neuroscience*, vol. 2020, pp. 1–15, May 2020, doi: 10.1155/2020/2630104.

[11] K. R. Devabalaji and K. Ravi, "Optimal size and siting of multiple DG and DSTATCOM in radial distribution system using Bacterial Foraging Optimization Algorithm," *Ain Shams Engineering Journal*, vol. 7, no. 3, pp. 959–971, Sep. 2016, doi: 10.1016/j.asej.2015.07.002.

[12] R. Roy, T. Das, and K. K. Mandal, "Optimal reactive power dispatch using a novel optimization algorithm," *Journal of Electrical Systems and Information Technology*, vol. 8, no. 1, p. 18, Dec. 2021, doi: 10.1186/s43067-021-00041-y.

[13] R. D. Zimmerman, C. E. Murillo-Sánchez, and R. J. Thomas, "MATPOWER: steady-state operations, planning, and analysis tools for power systems research and education," *IEEE Transactions on Power Systems*, vol. 26, no. 1, pp. 12–19, Feb. 2011, doi: 10.1109/TPWRS.2010.2051168.

[14] I. Musirin and T. K. Abdul Rahman, "Novel fast voltage stability index (FVSI) for voltage stability analysis in power transmission system," in *Student Conference on Research and Development*, IEEE, 2002, pp. 265–268. doi: 10.1109/SCORED.2002.1033108.

[15] O. D. Montoya, W. Gil-González, and L. F. Grisales-Noreña, "An exact MINLP model for optimal location and sizing of DGs in distribution networks: A general algebraic modeling system approach," *Ain Shams Engineering Journal*, vol. 11, no. 2, pp. 409–418, Jun. 2020, doi: 10.1016/j.asej.2019.08.011.

[16] K. M. Passino, "Biomimicry of Bacterial Foraging for Distributed Optimization and Control," *IEEE Control Systems*, vol. 22, no. 3, pp. 52–67, Jun. 2002, doi: 10.1109/MCS.2002.1004010.

[17] S. K. Patel *et al.*, "Graphene-based H-shaped biosensor with high sensitivity and optimization using ML-based algorithm," *Alexandria Engineering Journal*, vol. 68, pp. 15–28, Apr. 2023, doi: 10.1016/j.aej.2023.01.002.

[18] S. W. Mathenge, E. T. Mharakurwa, and L. Mogaka, "Cost-based optimal allocation of shunt capacitors in radial distribution networks considering load types using crow search algorithm," *Journal of Electrical and Computer Engineering*, vol. 2025, no. 1, Jan. 2025, doi: 10.1155/jece/9238961.

[19] B. Bhattacharyya and S. Raj, "Swarm intelligence based algorithms for reactive power planning with Flexible AC transmission system devices," *International Journal of Electrical Power and Energy Systems*, vol. 78, pp. 158–164, Jun. 2016, doi: 10.1016/j.ijepes.2015.11.086.

[20] Z. Qu *et al.*, "Dynamic exploitation Gaussian bare-bones bat algorithm for optimal reactive power dispatch to improve the safety and stability of power system," *IET Renewable Power Generation*, vol. 16, no. 7, pp. 1401–1424, May 2022, doi: 10.1049/rpg2.12428.

[21] F. S. Abu-Mouti and M. E. El-Hawary, "Optimal distributed generation allocation and sizing in distribution systems via artificial bee colony algorithm," *IEEE Transactions on Power Delivery*, vol. 26, no. 4, pp. 2090–2101, Oct. 2011, doi: 10.1109/TPWRD.2011.2158246.

[22] L. Shen, J. Chen, Z. Zeng, J. Yang, and J. Jin, "A novel echo state network for multivariate and nonlinear time series prediction," *Applied Soft Computing Journal*, vol. 62, pp. 524–535, Jan. 2018, doi: 10.1016/j.asoc.2017.10.038.

[23] S. A. Sani, G. A. Bakare, Y. S. Haruna, A. I. Isa, and U. Musa, "Optimal capacitor placement in distribution systems using improved bacterial foraging algorithm," in *2019 IEEE PES/IAS PowerAfrica*, IEEE, Aug. 2019, pp. 233–237. doi: 10.1109/PowerAfrica.2019.8928867.

[24] M. N. I. Sarkar, L. G. Meegahapola, and M. Datta, "Optimal reactive power dispatch considering reactive power support from renewable energy generators," in *2019 IEEE International Conference on Industrial Technology (ICIT)*, IEEE, Feb. 2019, pp. 667–672. doi: 10.1109/ICIT.2019.8755132.

[25] A. A. Abou El-Ela, R. A. El-Sehiemy, A. M. Kinawy, and M. T. Mouwafi, "Optimal capacitor placement in distribution systems for power loss reduction and voltage profile improvement," *IET Generation, Transmission and Distribution*, vol. 10, no. 5, pp. 1209–1221, Apr. 2016, doi: 10.1049/iet-gtd.2015.0799.

BIOGRAPHIES OF AUTHORS



Anh Tuan Bui is a lecturer in the Faculty of Engineering Technology at Phuong Dong University. He received his Engineer's and Master's degrees in Electrical Engineering from Hanoi University of Science and Technology in 2001 and 2006, respectively, and his Ph.D. degree in Electrical Engineering from Claude Bernard University Lyon 1, France, in 2012. Currently, his research interests include the characterization and modeling of soft magnetic materials, power quality improvement and energy-saving solutions, along with optimal control methods. He can be contacted at email: tuan.ba@phuongdong.edu.vn.



Tien Dung Nguyen received the M.S. and Ph.D. degrees in Control and Automation from Le Quy Don Technical University, Vietnam, in 2014 and 2024, respectively. He is currently a lecturer and researcher at the Faculty of Automation, Artificial Intelligence and Intelligent Systems, Electric Power University, Hanoi, Vietnam. His research interests include electric power quality improvement, embedded systems, robotics, and intelligent control. He can be contacted at email: dungnt@epu.edu.vn.



Tung Tran received the Engineer degree in Power Systems from Hanoi University of Science and Technology, Vietnam, in 2004, and the M.Eng. degree in Electrical Engineering from Thai Nguyen University of Technology, Thai Nguyen University, Vietnam, in 2008. He is currently a Lecturer with the Center for Practice and Laboratory, Electric Power University, Hanoi, Vietnam. His main research interests include power quality improvement and optimal control of power systems. He can be contacted at email: tungt@epu.edu.vn.